


An ultra-incompressible Mn_3N compound predicted by first-principles genetic algorithm

Cite as: J. Appl. Phys. **128**, 055112 (2020); <https://doi.org/10.1063/5.0014018>

Submitted: 15 May 2020 . Accepted: 24 July 2020 . Published Online: 06 August 2020

Chao Zhang , Yang Sun, Feng Zhang, Kai-Ming Ho, and Cai-Zhuang Wang



[View Online](#)



[Export Citation](#)



[CrossMark](#)

Lock-in Amplifiers
up to 600 MHz



An ultra-incompressible Mn_3N compound predicted by first-principles genetic algorithm

Cite as: J. Appl. Phys. 128, 055112 (2020); doi: 10.1063/5.0014018

Submitted: 15 May 2020 · Accepted: 24 July 2020 ·

Published Online: 6 August 2020



Chao Zhang,^{1,2}  Yang Sun,² Feng Zhang,² Kai-Ming Ho,^{2,3} and Cai-Zhuang Wang^{2,3,a)}

AFFILIATIONS

¹Department of Physics, School of Opto-electronic Information Science and Technology, Yantai University, Yantai 264005, China

²Ames Laboratory—USDOE, Iowa State University, Ames, Iowa 50011, USA

³Department of Physics and Astronomy, Iowa State University, Ames, Iowa 50011, USA

^{a)}Author to whom correspondence should be addressed: czwang@ameslab.gov

ABSTRACT

Using genetic algorithms for an unbiased structure search and first-principles total-energy calculations, a stable manganese nitride, Mn_3N , is discovered. Mn_3N is a nonmagnetic metal and isostructural to superhard Re_3N . Mn_3N exhibits a large bulk modulus and incompressibility comparable to that of the ultra-incompressible OsB. We show that the large bulk modulus can be attributed to the strong covalent bonding in this system. Phonon calculations and analysis confirm the dynamical stability of the Mn_3N compound. We also show that weak electron-phonon coupling leads to a small superconducting transition temperature for Mn_3N .

Published under license by AIP Publishing. <https://doi.org/10.1063/5.0014018>

I. INTRODUCTION

Transition metal nitrides form a compelling class of materials with a versatile electronic structure ranging from insulating to semiconducting to metallic and have been attracting considerable interest for many potential applications, including permanent magnets,¹ ceramic hard coatings,^{2,3} superconductors,^{4,5} photovoltaics,^{6,7} thermoelectrics,^{8,9} and piezoelectrics.¹⁰ Among these potential applications, using transition metal nitrides for superhard coatings is very promising due to their outstanding mechanical properties. The introduction of nitrogen atoms into the interstitial sites of transition metals with high valence-electron densities makes the compounds superhard and resistant to squeezing.¹¹ It has been shown, in general, that transition metal nitrides have larger bulk moduli than their parent metal, and bulk moduli are well correlated with the hardness of the materials.¹² For example, the experimentally measured bulk modulus of IrN_2 is about 428 GPa, which is 17% larger than that of pure Ir. Note that the bulk modulus of IrN_2 is very close to that of superhard diamond with a bulk modulus of 440 GPa.¹²

However, the discovery of transition metal nitrides is limited by the difficulties in their synthesis. The triply bonded di-nitrogen molecule, $\text{N}\equiv\text{N}$, displays one of the strongest chemical bonds, and thus N_2 gas is ultra-stable and has low reactivity at low temperatures. Solid-state nitrides generally have small formation energies

and tend to decompose at high temperatures. Therefore, transition metal nitrides must be synthesized under extreme conditions, such as high temperatures and high pressures.^{12–14} These stringent synthesis constraints, coupled with the poor intrinsic stabilities of nitrides, make the discovery of new transition metal nitrides difficult in the laboratory.

Theoretical structure prediction could help to tackle these problems and can play a crucially important role in the discovery of new materials. Several theoretical methods already have been developed for crystal structure prediction, such as simulated annealing,^{15–17} genetic algorithm (GA),¹⁸ random search,¹⁹ basin (or minima) hopping,²⁰ and particle swarm optimization.²¹ A timely feedback between theoretical structure prediction and experimental synthesis remarkably accelerates the discovery of new materials. Among these methods, an adaptive genetic algorithm (AGA) balances the accuracy of first-principles total-energy calculations and the speed of classical potential searches.²² This method has successfully predicted structures of various systems ranging from bulk systems (elemental solid to binary and ternary compounds) to interface.^{23–25} For transition metal nitrides, a predicted hexagonal Co_3N using the AGA method was successfully synthesized by experiments.²⁶ Additionally, a series of stable and metastable structures of transition metal nitrides has been predicted.^{27,28} Some of these structures have excellent magnetic

properties, providing useful insights into the development of rare-earth-free magnets.

In this work, a stable manganese nitride (Mn_3N) with excellent mechanical properties was predicted by combining a GA structure search with first-principles total-energy calculations. The resulting hexagonal Mn_3N exhibits a large bulk modulus and incompressibility. The hexagonal Mn_3N also satisfies the criteria of mechanical and thermodynamic stability.

II. COMPUTATIONAL METHODS

The search for low-energy crystalline structures of Mn_3N was performed via the GA technique as implemented in the AGA code,²² which is designed specifically for unbiased global structural searches using only the chemical compositions of the compounds. In the GA search, structural relaxations for the offspring structures at every GA generation are carried out by first-principles calculations within the framework of density functional theory (DFT) as implemented in the Vienna *Ab initio* Simulation Package (VASP).²⁹ In these DFT calculations, we adopt the Perdew–Burk–Ernzerhof (PBE) functional at the generalized gradient approximation (GGA)³⁰ level and projected-augmented wave (PAW)³¹ with $3p^6 3d^6 4s^1$, $4p^6 4d^6 5s^1$, $5p^6 5d^6 6s^1$, and $2s^2 2p^3$ as valence electrons for Mn, Re, Tc, and N atoms, respectively. A plane wave basis set with a kinetic energy cut-off of 600 eV is used to expand the electronic wave function and a uniform, Γ -centered k mesh³² with $2\pi \times 0.03 \text{ \AA}^{-1}$ spacing are used to perform the Brillouin zone integrations. All of the candidate structures are optimized with spin polarization until the net forces on each atom are below 1 meV/Å.

Phonon calculations are performed with a supercell approach. Real-space force constants of a $3 \times 3 \times 1$ supercell of Mn_3N are calculated by the small atomistic displacement method through VASP, interfaced with the PHONOPY code.³³ The electron–phonon coupling (EPC) is calculated using the Quantum-Espresso (QE) code³⁴ with the PBE functional and PAW pseudopotentials. The plane wave basis set and the charge density are expanded with the kinetic energy cut-offs of 100 and 600 Ry, respectively, in the EPC

calculations. The EPC matrix elements are computed on a $6 \times 6 \times 2$ q -points mesh using individual EPC matrices obtained with a $24 \times 24 \times 8$ k -points mesh.

III. RESULTS AND DISCUSSION

Using only the knowledge of the chemical compositions, our structure search scheme correctly reproduced the experimental known manganese nitrides, namely, Mn_4N , Mn_2N , Mn_3N_2 , MnN , and Mn_3N_4 . This accomplishment validates the GA method used in the structural searches of Mn–N systems. From our GA searches of Mn_3N , a hexagonal structure with a space group of $P\bar{6}m2$ (No. 187) was discovered to have the lowest energy, as shown on the right side of Fig. 1. This can be seen from the convex hull for the Mn–N system shown on the left side of Fig. 1. The convex hull is constructed using experimental reported structures of Mn_2N and MnN and our predicted hexagonal structure of Mn_3N . The lowest-energy crystalline structure of elemental Mn (space group $I\bar{4}3m$)³⁵ and that of N (space group $Pa\bar{3}$)³⁶ is used as a reference for the formation energy calculations. Based on the discovery of the Mn_3N compound from our structure search, we assert that the ferromagnetic Mn_4N is actually metastable with a formation energy is approximately 14.8 meV/atom above the tie-line connecting the Mn and Mn_3N phases in the convex hull construction. The antiferromagnetic Mn_3N_2 almost lies on the convex hull and the formation energy of an N-rich Mn_3N_4 compound is approximately 142 meV/atom above the convex hull.

The hexagonal Mn_3N structure is a nonmagnetic compound with only one formula unit in the conventional cell, whose prototype is hexagonal Re_3N (space group $P\bar{6}m2$). The optimized lattice parameters of Mn_3N are $a = 2.587 \text{ \AA}$ and $c = 6.399 \text{ \AA}$ at ambient pressure and 0 K. The Mn1 and Mn2 atoms occupy the Wyckoff position $2h$ (0.3333, 0.6667, and 0.1960) and $1f$ (0.6667, 0.3333, and 0.5), respectively, whereas the N atom takes the Wyckoff position $1e$ (0.6667, 0.3333, and 0.0). One N atom is coordinated by eight Mn2 atoms in a triangular prism arrangement. These N-centered triangular prisms share edges with each other

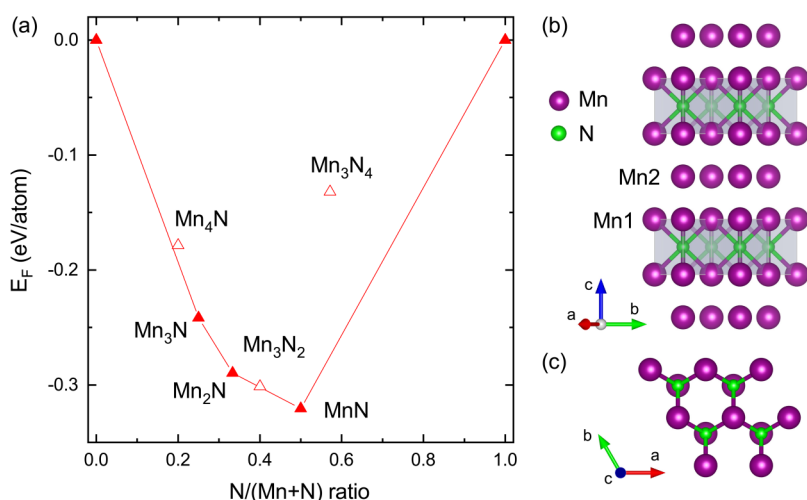


FIG. 1. (a) Formation energy of convex hull of the Mn–N system. The formation energies are calculated as $E_F(\text{Mn}_x\text{N}_{1-x}) = E(\text{Mn}_x\text{N}_{1-x}) - xE(\text{Mn}) - (1-x)E(\text{N})$, where $0 \leq x \leq 1$ and energies of bcc Mn and N are used as references. (b) Side and (c) top views of the crystal structure of hexagonal Mn_3N .

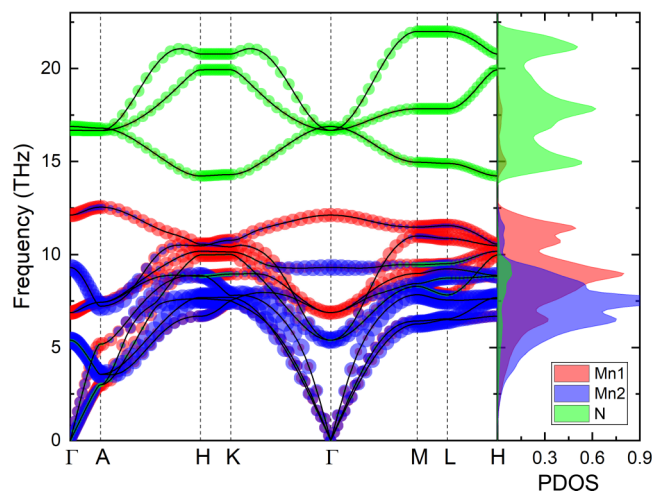


FIG. 2. Phonon band structure and projected density of states for hexagonal Mn_3N .

propagating along the ab plane and are intercalated by one-layer Mn1 atoms forming a three-dimensional structure. The intralayer distance between Mn1 layer and Mn2 layer is 1.945 Å, and the interatomic distance of Mn–Mn distances in the Mn1 layer and Mn2 layer are 2.587 and 2.453 Å, respectively.

The dynamical stability of the hexagonal Mn_3N is established via phonon calculations. The absence of imaginary frequencies confirms dynamical stability of the predicted Mn_3N , as shown in Fig. 2. Due to the fact that Mn is much heavier than N, the vibration frequencies of Mn atoms are apparently lower than those of N atoms. Therefore, there is a gap of 2.0 THz, which divides the phonon band structure into two major groups. Above the gap, the relatively lighter N atoms dominate the high-frequency region with a bandwidth of 7.7 THz. The vibration modes of Mn1 atom range from 2.5 to 12.5 THz with the main peak in projected density of states (PDOS) centered at 9 THz. By comparison, the vibration band of the layered Mn2 atoms is significantly narrower and centered at a lower frequency of about 7.5 THz. The difference between the vibration properties of the Mn1 and Mn2 atoms can be attributed to the interaction of the Mn1 atoms with the N atoms.

Since hexagonal Re_3N , the prototype of Mn_3N , has excellent mechanical properties,¹⁴ it is worth to investigate the mechanical properties of Mn_3N . The elastic stiffness constants, various moduli, Pugh's ratio, and Poisson's ratio of Mn_3N , as well as Tc_3N and Re_3N are calculated and compared, as listed in Table I. The elastic stiffness constants of Mn_3N satisfy the mechanical stability criteria³⁹ $C_{11} > |C_{12}|$, $2C_{13}^2 < C_{33}(C_{11} + C_{12})$, $C_{44} > 0$, and $C_{66} = (C_{11} - C_{12}) > 0$. The mechanical stability of Mn_3N is consistent with the dynamical stability derived from phonon calculations. The elastic stiffness constants C_{11} and C_{33} reflect the stiffness to uniaxial strains along the crystallographic a axis and c axis, respectively. C_{33} is larger than C_{11} , suggesting that Mn_3N is much stiffer along the c axis than the a axis. Among the three transition metal nitrides, Re_3N possesses the largest elastic stiffness constants, and the values of C_{11} , C_{33} , and C_{44} for Re_3N are approximately 1.16, 1.11, and 1.09 times of that for Mn_3N .

Based on Voigt–Reuss–Hill (VRH) approximation,^{40–42} the bulk moduli of Mn_3N , Tc_3N , and Re_3N are 307, 332, and 389 GPa, respectively. The calculated B of Re_3N in this work deviates 1.5% of the experimental value and is in agreement with the previous theoretical results.^{14,38} Although B of Mn_3N is 21.1% smaller than that of superhard Re_3N , the relatively large B implies that Mn_3N is incompressible. It is worth noting that Mn_3N and Re_3N have similar values of shear modulus G , which is a qualitative predictor of hardness of a material. B is systematically larger than G for all three nitrides. This trend also is found in other Re–N and Tc–N systems.^{37,38,43–45} Furthermore, the B/G ratio proposed by Pugh can provide information about the ductile–brittle nature of a material.⁴⁶ According to Pugh's simple rule, if $B/G > 1.75$, then the material behaves in a ductile manner; otherwise, the material is brittle. It is interesting that Mn_3N shows some degree of brittleness with a Pugh's ratio of 1.597, whereas Tc_3N and Re_3N exhibit ductile characteristics due to the larger Pugh's ratio. Young's modulus E is a measure of the stiffness of a material; a larger E value indicates stiffer material. Thus, the stiffness of the three nitrides is $\text{Re}_3\text{N} > \text{Mn}_3\text{N} > \text{Tc}_3\text{N}$. For Poisson's ratio ν , the values for the three compounds are within the range from 0.24 to 0.45 for typical metals.

To further investigate the incompressibility of Mn_3N , the pressure-dependent relative volume is shown in Fig. 3(a). For the purposes of comparison, the calculation results for super-hard diamond, ultra-incompressible OsB, Re_3N , and Tc_3N are also plotted. It is evident from the plot that although the incompressibility of Mn_3N is lower than that of super-hard diamond, its

TABLE I. Elastic stiffness constants C_{ij} (GPa), bulk modulus B (GPa), shear modulus G (GPa), Young's modulus E (GPa), Pugh's ratio B/G , and Poisson's ratio ν .

	C_{11}	C_{33}	C_{44}	C_{12}	C_{13}	B	G	E	B/G	ν	Reference
Mn_3N	557	690	172	183	150	307	192	477	1.597	0.241	This work
Tc_3N	546	658	167	191	217	332	177	451	1.874	0.274	This work
	495					318	153	396	2.078	0.290	GGA ³⁷
Re_3N	647	763	188	206	264	389	207	527	1.882	0.274	This work
	657	845	198	248	244	399	213	543	1.878	0.274	GGA ³⁸
						413					GGA ¹⁴
						395					Expt. ¹⁴

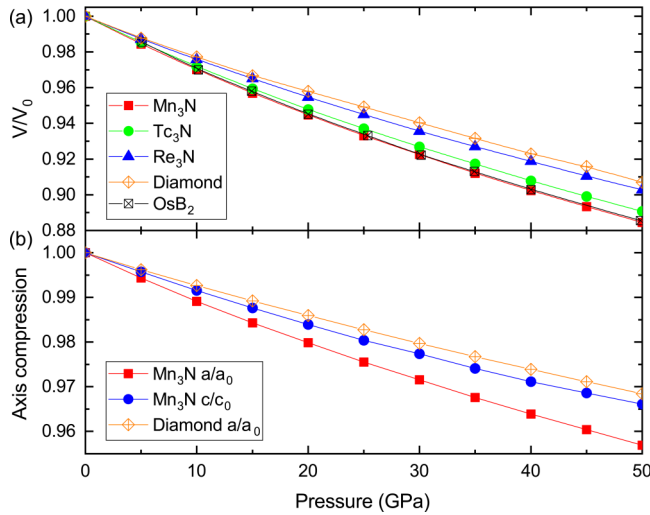


FIG. 3. (a) Volume as a function of pressure with respect to the equilibrium volume V_0 . (b) Axial compression as a function of pressure with equilibrium lattice constants a_0 and c_0 .

compressible curve coincides with the ultra-incompressible material, OsB .⁴⁷ Thus, the predicted hexagonal Mn_3N can be a potential ultra-incompressible material with excellent mechanical properties. As shown in Fig. 3(a), Re_3N and Tc_3N also have remarkable incompressibility. There is a large difference in the compressibility between the a and c axes. The fractional axis compression as a function of pressure for Mn_3N and diamond is shown in Fig. 3(b). For hexagonal Mn_3N , the c axis is more incompressible than the a axis, consistent with the evidence discussed above that C_{33} is larger than C_{11} . The compressibility along the c axis has a comparable value to that of diamond. The c axis compressibility of Mn_3N and the a axis compressibility of diamond are 0.966 and 0.968 at 50 GPa, respectively, whereas the a axis compressibility of Mn_3N has a relatively small value (0.957) at 50 GPa.

Apart from the anisotropy evidenced in the compression of axes, several indexes, including percent anisotropy (A_B and A_G), have been developed to evaluate mechanical anisotropy.^{48,49} The present anisotropy in compressibility and shear are defined as follows: $A_B = (B_V - B_R)/(B_V + B_R)$ and $A_G = (G_V - G_R)/(G_V + G_R)$, where the subscripts V and R denote the Voigt and Reuss bounds, respectively. For a completely isotropic system, A_B and A_G are 0, and the deviation from 0 measures the degree of elastic anisotropy. A_B and A_G for the hexagonal Mn_3N are 0.002 and 0.010, respectively, indicating a weak elastic anisotropy.

To understand the nature of the mechanical properties of Mn_3N , the underlying electronic structures have been analyzed. The electronic projected density of states (PDOS) of Mn_3N , Tc_3N , and Re_3N are displayed in Fig. 4. The valence and conduction bands near the Fermi level are mainly contributed by the transition metal d electrons with strongly hybridized N $2p$ electrons, and the DOS at the Fermi level for the Mn_3N , Tc_3N , and Re_3N are 2.983,

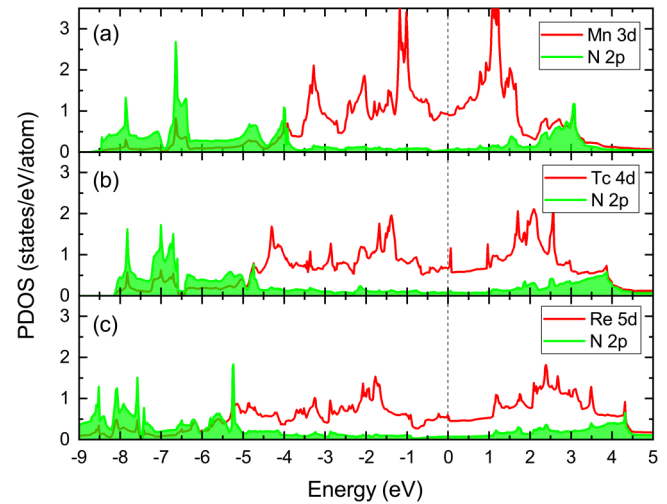


FIG. 4. Electronic projected density of states for (a) Mn_3N , (b) Tc_3N , and (c) Re_3N . Vertical lines indicate the Fermi level.

2.337, and 2.206 states/eV/f.u., respectively. These values show that all three nitrides are metals. The N $2p$ electrons dominate the energy from -8 to -4 eV. Thus, the chemical bonding in these nitrides is a mixture of metallic and covalent characters. The degree of covalent component correlates with the bulk modulus and thus hardness of these materials.⁵⁰ In the energy range of -5 to 1.5 eV, the PDOS of Mn $3d$ electrons for Mn_3N is significantly larger than that of Tc $4d$ and Re $5d$ electrons, whereas the PDOS of N $2p$ electrons for Mn_3N is slightly smaller than that in Re_3N . These results demonstrate that the covalent bonding strength of Mn_3N is smaller than that of Re_3N , where the transition metal mass is larger. This result is consistent with the bulk modulus trend mentioned above, i.e., $\text{Mn}_3\text{N} < \text{Re}_3\text{N}$.

The electron-phonon coupling parameters (λ) of these three nitrides have been calculated to check the possible superconducting properties. The electron-phonon coupling of Mn_3N , Tc_3N , and Re_3N are 0.326, 0.469, and 0.455, respectively. The superconducting transition temperature (T_c) is estimated using the McMillan equation modified by Allen and Dynes:⁵¹ $T_c = \frac{\omega_{\log}}{1.2} \exp\left[-\frac{1.04(1+\lambda)}{\lambda - \mu^*(1+0.62\lambda)}\right]$, where ω_{\log} is the logarithmic average phonon frequency and μ^* is the Coulomb pseudopotential. The relatively small λ values result in T_c of 0.41, 3.08, and 2.26 K for Mn_3N , Tc_3N , and Re_3N , respectively.

IV. CONCLUSION

A nonmagnetic Mn-N compound, Mn_3N , has been predicted by utilizing first-principles calculations and the GA method. The Mn_3N compound has hexagonal symmetry and is isostructural to superhard Re_3N . The five independent elastic stiffness constants satisfy the Born-Huang mechanical stability criteria. Based on the VRH approximation, Mn_3N possesses a large bulk modulus of 307 GPa originating from the Mn $3d$ and N $2p$ hybridization. Its

incompressibility is similar to the ultra-incompressible OsB. The c axis is more incompressible than the a axis. The phonon calculations establish the dynamical stability of Mn_3N . The weak electron-phonon coupling strength results in a low superconducting T_c (0.42 K) for Mn_3N .

ACKNOWLEDGMENTS

Chao Zhang acknowledges financial support from the National Natural Science Foundation of China (NNSFC) (Grant No. 11874318) and the Natural Science Foundation of Shandong Province (Grant No. ZR2018MA043). Work at Ames Laboratory was supported by the U.S. Department of Energy (DOE), Office of Science, Basic Energy Sciences, Division of Materials Sciences and Engineering, including the computer time support on National Energy Research Scientific Computing Center (NERSC) in Berkeley, CA. The Ames Laboratory is operated for the DOE by Iowa State University under Contract No. DE-AC02-07CH11358.

DATA AVAILABILITY

The data that support the findings of this study are available within the article.

REFERENCES

- ¹Y. Sugita, K. Mitsuoka, M. Komuro, H. Hoshiya, Y. Kozono, and M. Hanazono, *J. Appl. Phys.* **70**, 5977 (1991).
- ²Z. Peng, H. Miao, L. Qi, S. Yang, and C. Liu, *Acta Mater.* **51**, 3085 (2003).
- ³S. Vepřek and S. Reiprich, *Thin Solid Films* **268**, 64 (1995).
- ⁴X.-J. Chen, V. V. Struzhkin, Z. Wu, M. Somayazulu, J. Qian, S. Kung, A. N. Christensen, Y. Zhao, R. E. Cohen, H.-K. Mao, and R. J. Hemley, *Proc. Natl. Acad. Sci. U.S.A.* **102**, 3198 (2005).
- ⁵S. Yamanaka, K. Hotehama, and H. Kawaji, *Nature* **392**, 580 (1998).
- ⁶L. Yulianti, J.-H. Yang, X. Wang, K. Maeda, T. Takata, M. Antonietti, and K. Domen, *J. Mater. Chem.* **20**, 4295 (2010).
- ⁷A. Zakutayev, *J. Mater. Chem. A* **4**, 6742 (2016).
- ⁸I. Ohkubo and T. Mori, *Chem. Mater.* **26**, 2532 (2014).
- ⁹C. X. Quintela, F. Rivadulla, and J. Rivas, *Appl. Phys. Lett.* **94**, 152103 (2009).
- ¹⁰C. Tholander, C. B. A. Andersson, R. Armiento, F. Tasnádi, and B. Alling, *J. Appl. Phys.* **120**, 225102 (2016).
- ¹¹R. B. Kaner, J. J. Gilman, and S. H. Tolbert, *Science* **308**, 1268 (2005).
- ¹²A. F. Young, C. Sanloup, E. Gregoryanz, S. Scandolo, R. J. Hemley, and H. Mao, *Phys. Rev. Lett.* **96**, 155501 (2006).
- ¹³J. C. Crowhurst, A. F. Goncharov, B. Sadigh, C. L. Evans, P. G. Morrall, J. L. Ferreira, and A. J. Nelson, *Science* **311**, 1275 (2006).
- ¹⁴A. Friedrich, B. Winkler, L. Bayarjargal, W. Morgenroth, E. A. Juarez-Arellano, V. Milman, K. Refson, M. Kunz, and K. Chen, *Phys. Rev. Lett.* **105**, 085504 (2010).
- ¹⁵K. Doll, J. C. Schön, and M. Jansen, *Phys. Chem. Chem. Phys.* **9**, 6128 (2007).
- ¹⁶S. Kirkpatrick, C. D. Gelatt, and M. P. Vecchi, *Science* **220**, 671 (1983).
- ¹⁷L. T. Wille, *Nature* **324**, 46 (1986).
- ¹⁸D. M. Deaven and K. M. Ho, *Phys. Rev. Lett.* **75**, 288 (1995).
- ¹⁹C. J. Pickard and R. J. Needs, *Phys. Rev. Lett.* **97**, 045504 (2006).
- ²⁰S. Goedecker, *J. Chem. Phys.* **120**, 9911 (2004).
- ²¹Y. Wang, J. Lv, L. Zhu, and Y. Ma, *Phys. Rev. B* **82**, 094116 (2010).
- ²²S. Q. Wu, M. Ji, C. Z. Wang, M. C. Nguyen, X. Zhao, K. Umemoto, R. M. Wentzcovitch, and K. M. Ho, *J. Phys. Condens. Matter* **26**, 035402 (2013).
- ²³X. Zhao, Q. Shu, M. C. Nguyen, Y. Wang, M. Ji, H. Xiang, K.-M. Ho, X. Gong, and C.-Z. Wang, *J. Phys. Chem. C* **118**, 9524 (2014).
- ²⁴X. Zhao, M. C. Nguyen, W. Y. Zhang, C. Z. Wang, M. J. Kramer, D. J. Sellmyer, X. Z. Li, F. Zhang, L. Q. Ke, V. P. Antropov, and K. M. Ho, *Phys. Rev. Lett.* **112**, 045502 (2014).
- ²⁵M. Ji, K. Umemoto, C.-Z. Wang, K.-M. Ho, and R. M. Wentzcovitch, *Phys. Rev. B* **84**, 220105 (2011).
- ²⁶B. Balasubramanian *et al.*, *Nanoscale* **10**, 13011 (2018).
- ²⁷X. Zhao, L. Ke, C.-Z. Wang, and K.-M. Ho, *Phys. Chem. Chem. Phys.* **18**, 31680 (2016).
- ²⁸X. Zhao, C.-Z. Wang, Y. Yao, and K.-M. Ho, *Phys. Rev. B* **94**, 224424 (2016).
- ²⁹G. Kresse and J. Furthmüller, *Phys. Rev. B* **54**, 11169 (1996).
- ³⁰J. P. Perdew, K. Burke, and M. Ernzerhof, *Phys. Rev. Lett.* **77**, 3865 (1996).
- ³¹G. Kresse and D. Joubert, *Phys. Rev. B* **59**, 1758 (1999).
- ³²H. J. Monkhorst and J. D. Pack, *Phys. Rev. B* **13**, 5188 (1976).
- ³³A. Togo and I. Tanaka, *Scr. Mater.* **108**, 1 (2015).
- ³⁴P. Giannozzi *et al.*, *J. Phys. Condens. Matter* **21**, 395502 (2009).
- ³⁵J. A. Oberteuffer and J. A. Ibers, *Acta Crystallogr. Sect. B* **26**, 1499 (1970).
- ³⁶J. Donohue, *Acta Crystallogr.* **14**, 1000 (1961).
- ³⁷P. F. Weck, E. Kim, and K. R. Czerwinski, *Dalton Trans.* **40**, 6738 (2011).
- ³⁸V. V. Bannikov, I. R. Shein, and A. L. Ivanovskii, *Phys. Status Solidi B* **248**, 1369 (2011).
- ³⁹F. Mouhat and F.-X. Coudert, *Phys. Rev. B* **90**, 224104 (2014).
- ⁴⁰W. Voigt, *Lehrbuch der Kristallphysik* (Teubner, Leipzig, 1928).
- ⁴¹A. Reuss, *Z. Angew. Math. Mech.* **9**, 49 (1929).
- ⁴²R. Hill, *Proc. Phys. Soc. Sect. A* **65**, 349 (1952).
- ⁴³Y. Liang, C. Li, W. Guo, and W. Zhang, *Phys. Rev. B* **79**, 024111 (2009).
- ⁴⁴Y. Li and Z. Zeng, *Chem. Phys. Lett.* **474**, 93 (2009).
- ⁴⁵Y.-L. Li and Z. Zeng, *Solid State Commun.* **149**, 1591 (2009).
- ⁴⁶S. F. Pugh, *London, Edinburgh, Dublin Philos. Mag. J. Sci.* **45**, 823 (1954).
- ⁴⁷R. W. Cumberland, M. B. Weinberger, J. J. Gilman, S. M. Clark, S. H. Tolbert, and R. B. Kaner, *J. Am. Chem. Soc.* **127**, 7264 (2005).
- ⁴⁸P. Ravindran, L. Fast, P. A. Korzhavyi, B. Johansson, J. Wills, and O. Eriksson, *J. Appl. Phys.* **84**, 4891 (1998).
- ⁴⁹D. H. Chung and W. R. Buessem, *J. Appl. Phys.* **38**, 2010 (1967).
- ⁵⁰S.-H. Jhi, J. Ihm, S. G. Louie, and M. L. Cohen, *Nature* **399**, 132 (1999).
- ⁵¹P. B. Allen and R. C. Dynes, *Phys. Rev. B* **12**, 905 (1975).